Birkbeck
UNIVERSITY OF LONDON

BIROn - Birkbeck Institutional Research Online

Alexander, Louise and Snape, Joshua F. and Crawford, Ian and Joy, K.H. and Downes, Hilary (2014) Searching for nonlocal lithologies in the Apollo 12 regolith: a geochemical and petrological study of basaltic coarse fines from the Apollo lunar soil sample 12023,155. Meteoritics & Planetary Science 49 (7), pp. 1288-1304. ISSN 1086-9379.

Downloaded from: https://eprints.bbk.ac.uk/id/eprint/11020/

Usage Guidelines:
Please refer to usage guidelines at https://eprints.bbk.ac.uk/policies.html or alternatively contact lib-eprints@bbk.ac.uk.

Searching for non-local lithologies in the Apollo 12 regolith: A geochemical and petrological study of basaltic coarse fines from the Apollo lunar soil sample 12023,155

Louise Alexander[1, 2], Joshua F. Snape[2, 3, 4], Ian A. Crawford[1, 2], Katherine H. Joy[3, 5], and Hilary Downes[1, 2].

1. Department of Earth and Planetary Science, Birkbeck College, University of London, Malet Street, London, WC1E 7HX, UK.(l.alexander@bbk.ac.uk).
2. The Centre for Planetary Sciences at UCL-Birkbeck, Gower Street, London WC1E 6BT, UK.
3. Department of Earth Sciences, University College London, Gower Street, London, WC1E 6BT, UK,
4. Department of Physical Sciences, Open University, Milton Keynes, MK7 6AA, UK.
5. School of Earth, Atmospheric and Environmental Sciences, University of Manchester, Oxford Road, Manchester, M13 9PL, UK.

Keywords: mare-basalt, lunar-regolith, Apollo 12, lunar-volcanism, LA-ICP-MS

Running header: Apollo 12 regolith basalt fragments

Abstract

New data from a petrological and geochemical examination of 12 coarse basaltic fines from the Apollo 12 soil sample 12023,155 provide evidence of additional geochemical diversity at the landing site. In addition to the bulk chemical composition, major, minor and trace element analyses of mineral phases are employed to ascertain how these samples relate to the Apollo 12 lithological basalt groups, thereby overcoming the problems of representativeness of small samples. All of the samples studied are low-Ti basalts (0.9 – 5.7 wt% TiO_2), and many fall into the established olivine, pigeonite and ilmenite classification of Apollo 12 basaltic suites. There are five exceptions: sample 12023,155_1A is mineralogically and compositionally distinct from other Apollo 12 basalt types, with low pigeonite REE concentrations and low Ni (41 to 55 ppm) and Mn (2400 to 2556 ppm) concentrations in olivine. Sample 12023,155_11A is also unique, with Fe-rich mineral compositions and low bulk Mg# (=100 x atomic Mg/(Mg+Fe)) of 21.6. Sample 12023,155_7A has different plagioclase chemistry and crystallisation trends as well as a wider range of olivine Mg# (34-55) compared with other Apollo 12 basalts, and shows greater similarities to Apollo 14 high-Al basalts. Two other samples (12023,155_4A and _5A) are similar to the Apollo 12 feldspathic basalt 12038, providing additional evidence that feldspathic basalts represent a lava flow proximal to the Apollo 12 site rather than material introduced by impacts. We suggest that at least one, and possibly as many as four, separate parent magmas are required in addition to the previously identified olivine, pigeonite and ilmenite basaltic suites to account for the observed chemical diversity of basalts found in this study.

1. Introduction

Petrological and geochemical studies of lunar mare basalt samples have shown a diverse range of textures and chemistries (e.g., James and Wright, 1972; Papike et al., 1976, 1991, 1998; Rhodes et al., 1977; Baldridge et al., 1979; Taylor et al., 1991; Vaniman et al., 1991; Neal et al., 1994a, 1994b), providing valuable information about the complexity of basaltic volcanism on the Moon, and the composition and temporal evolution of the lunar mantle (e.g., Neal et al.,1994b; Snyder et al., 1997; Shearer et al., 2006). Here we are concerned with results from the Apollo 12 mission, which returned 34.3 kg of samples (LSPET, 1970; Vaniman et al., 1991).

Detailed high-resolution photogeologic mapping and crater size-frequency distribution measurements (Schultz and Spudis, 1983; Wilhelms, 1987; Hiesinger et al., 2000, 2003, 2010) indicate that a large number of individual basalt flows, including some of the youngest basalts (~1.2 Ga) on the Moon, occur in the Oceanus Procellarum region (Hiesinger et al., 2010). The location of the Apollo 12 landing site (3.2^0N, 23.4^0W) is within the eastern region of Oceanus Procellarum, and thus there has been potential for lateral transport of material across the

lunar surface by impact processes to this site (e.g., Li and Mustard, 2005; Zeigler et al., 2006; Petro and Pieters, 2007). It is, therefore, possible that some young basaltic material, exotic to the landing site, may have been sampled by the Apollo 12 mission. Constraining the extent of basaltic diversity at the Apollo 12 site, including the identification of such exotic material, would facilitate the study of lunar mantle processes and basalt petrogenesis that are key lunar science goals (NRC, 2007).

As part of our wider study of basaltic diversity in Oceanus Procellarum (see discussion by Crawford et al., 2007; Snape et. al., 2014), we here provide the results of a petrological and geochemical examination of basaltic fines from the Apollo 12 soil sample 12023,155, consisting of 12 coarse fines ~2 mm in diameter. Sample 12023 is a typical submature-mature lunar soil (I_s/FeO = 60: Becker and Clayton, 1978), collected from the bottom of a 20 cm deep trench on the eastern edge of Sharp Crater. This was one of the freshest craters sampled by the Apollo 12 mission, as indicated by high albedo material distributed around the rim (Shoemaker et al., 1970) and a wide range of exposure ages, mostly <500 Ma (Levine et al., 2005).

Most basalts from the Apollo 12 site have low-Ti compositions (1-6 wt% TiO_2 using the classification of Neal and Taylor, 1992) and can be grouped into the well-established lithological suites of pigeonite, olivine and ilmenite basalts on the basis of their mineralogy and bulk composition (James and Wright, 1972; Rhodes et al., 1977; Neal et al., 1994a).

Ilmenite basalts are considered to have been derived from a distinct mantle source region, while olivine and pigeonite basalts may have originated from a similar, shallower source region, with subsequent crustal assimilation accounting for differences between them (Snyder et al., 1997). In addition, there is a separate group of feldspathic basalts with high modal abundances of plagioclase (>38.5% by mode) and unique isotopic signatures (Nyquist et al., 1979, 1981). However, there is currently only one Apollo 12 sample (12038) assigned to this group (Beaty et al., 1979; Nyquist et al., 1979, 1981; Neal et al., 1994a). This has led to the suggestion that 12038 may not represent a lithology local to the Apollo 12 site, but may have been introduced to the area by impact mixing processes (Neal et al., 1994a).

A potentially serious problem with bulk chemistry classification for lunar samples is the small amount of material available, meaning that many samples analysed are not necessarily representative of their parent rocks. This is well documented (e.g., Rhodes et al., 1976; Neal and Taylor, 1992; Neal et al., 1994a; Snape et al., 2014). For example, Korotev et al. (2011) found that 39% of the basaltic soil fragments (2 to 4 mm size range) that they studied from the Apollo 12 site had compositions that were unrepresentative of the main lava flows (i.e., olivine, ilmenite and pigeonite) found in the area. Therefore, future studies of Apollo basalts and basaltic regolith fragments need to address this issue by looking at new ways to distinguish between basalt types. Our study will compare compositional and mineralogical data from the basaltic fines with other basalts from the Apollo 12 mission in order to determine how they fit into the recognised lithological groups and classification schemes, if at all. In addition to the bulk chemistry, we use major, minor and trace element chemistry in mineral phases to ascertain how these samples relate to the existing Apollo 12 lithological basalt groups, thereby overcoming the problems of representativeness of small samples. This work follows previous analyses of other Apollo 12 fines by Snape et al. (2014) and we have also indicated the textural classification used in that work in the description of samples here.

2. Analytical Methods

The samples studied were provided on loan from the curatorial facility at the Johnson Space Center (JSC). Eleven basalt grains were selected from the bulk 12023,155 regolith sample at the JSC curation laboratory, but twelve were received when the samples were mailed, indicating that one had broken in transit from the US to the UK (this sample is identified below).

Samples were weighed, photographed and assigned individual sample numbers (12023,155_1 to 12). All samples were then split in two using either a 213 nm laser and scalpel (samples 12023,155_2, 3, 4 and 5) or a scalpel only (samples 12023,155_1, 6, 7, 8, 9, 10, 11 and 12). The larger splits were designated 155_1A, etc., and used for petrographic analysis, while the smaller splits (155_1B, etc.) were kept aside for future radiometric dating. The A splits were mounted in epoxy resin and polished with alcohol-based lubricant and diamond paste, cleaned with isopropanol and coated with carbon.

Textures were examined using a JEOL JXA-8100 electron microprobe with an Oxford Instruments INCA energy dispersive system (EDS) operating at 15 keV accelerating voltage with a current of 10 nA to produce backscattered electron (BSE) images and elemental X-ray maps. The elemental maps were combined using the GNU Image Manipulation Program (GIMP) following the method described by Joy et al. (2006, 2008, 2011) and Snape et al. (2011a,b). Modal mineralogies were calculated from BSE images and elemental X-ray maps using imaging software (Adobe Photoshop) to identify the phases based on differences in tone, and the pixels corresponding to each phase were counted to establish the percentage of phases present. This method of determining modal mineralogy has been tested on previously studied Apollo samples and found to be in good agreement with published values (Snape et al., 2011b).

Major and minor element mineral analyses were obtained using a JEOL JXA 8100 Superprobe wavelength dispersive system (WDS) with an accelerating voltage of 15 keV, current of 25 nA and a beam diameter of 1 µm. The peak counting times were 20 s with a background measurement time of 10 s for most elements with the exception of Na for which the peak counting times were 10 s on peak and 5 s for the background. Analyses were calibrated against standards of natural silicates, oxides and Specpure® metals with data corrected using a ZAF program and additional corrections applied for Fe/Co and Ti/V peak overlaps. Errors were calculated from repeated measurements of BCR-2 USGS basaltic glass (USGS, 2009).

Bulk compositions were calculated by performing multiple EDS raster beam analyses (RBA) across the samples for 480 s count time at 15 keV. Such methods have previously been employed to assess sample or clast bulk composition by Joy et al. (2010) and Snape et al. (2011a, b,c, 2014). Samples were divided into approximately equal areas in order to fit into the field of view of the electron microprobe and five RBA of each area were completed, which were normalised to 100%, and averaged together. The averages of these RBA were weighted according to their relative surface areas. The areas of the RBA were determined using pixel counting with imaging software (Adobe Photoshop). Errors quoted for the bulk compositions are 1σ standard deviations of the five individual RBA analyses.

It is known that there are inaccuracies with the above method and, in addition to standard ZAF corrections, a correction needs to be applied to account for the difference in phase densities in the sample. Corrections were applied in accordance with the method of Warren (1997). This method has been previously tested on known lunar samples (Snape et al., 2011b) and found to be in good agreement with previously published bulk compositions.

Trace element analyses in mineral phases were obtained using laser ablation inductively coupled plasma mass spectrometry (LA-ICP-MS). The instrument used was an Agilent 7700X series ICP-MS coupled to a UP-213 New Wave Research laser. The pulse frequency was 10 Hz. Data were collected for 60 s, during which time the abundances of 34 elements were monitored. Background conditions were monitored for 30 s and the sample was ablated for 30 s with a laser spot size of 40 µm.

LA-ICP-MS data were reduced using the GEMOC Glitter software program (http://www.glitter-gemoc.com/), and Ca was used as the internal standard for pyroxene and plagioclase by comparing CaO wt% in minerals previously determined by WDS microprobe analysis. Manganese (MnO) was used as the internal standard for olivine. Analyses of pyroxene and plagioclase were externally calibrated with NIST 612 doped synthetic glass, and analyses of olivine were externally calibrated with NIST 610 doped synthetic glass (Pearce et al., 1997) under the same conditions as for sample analysis (i.e., maintaining a constant laser spot size). The NIST 610 was monitored as an unknown for pyroxene and plagioclase and NIST 612 was monitored as an unknown for olivine. Repeatability of the NIST 612 standard measurements over all measurement sessions has a total relative standard error range of between 0.03% and 0.26% for all elements analysed. Accuracy of the NIST 612 standard measurements to NIST 612 published values (Pearce et al., 1997) has a relative difference range of between -4.64% and +5.32% for all elements analysed (with the exception of Ni (+10.84%) and Ta (-10.37%)) and was typically <±0.66%; the larger errors on Ni are partly due to the use of Ni scatter cones in the ICP-MS instrument. Repeatability of the NIST 610 standard measurements over all measurement sessions has a total relative standard deviation range of between 0.03 and 0.14% for all elements analysed and was typically <0.07%. Accuracy of the NIST 610 standard measurements to published values (Pearce et al., 1997) has a relative difference range of -6.48% to +7.44% for all elements analysed but was typically <1.4%.

3. Results

3.1. Petrography

The samples are all unbrecciated holocrystalline basalts (Figs. 1 and 2). Their modal mineralogies are given in Table 1 and individual sample descriptions are given below. We compare the textures of the 12023 basaltic regolith chips to those from the 12003 soil sample studied and classified into different textural and chemical groups by Snape et al. (2014). According to this scheme Type 1 are subophitic to variolitic, Type 2 are ophitic with more tabular plagioclase, Types 3 and 4 are coarser grained with mostly mafic mineralogies, and the Type 4 samples containing more abundant olivine than Type 3.

Samples 155_3A, 4A, 5A, 9A, 11A and 12A are all textural Type 1 in accordance with the basaltic textural types of Snape et al. (2014). Sample 155_3A (1.5 x 1.1 mm) is sub-ophitic, consisting of strongly zoned pyroxene (48%), partially enclosing elongate, branching plagioclase laths (45%) up to 900 µm in length. Acicular ilmenite laths (4%) up to 600 µm in length cross-cut the silicates. Minor interstitial silica (4%) and phosphates (20 µm in diameter) are also present.

Sample 155_4A (1.0 x 0.9 mm, Fig. 1) consists of fractured, zoned pyroxene crystals (41%) 150 to 200 µm in size, together with a high modal abundance of blocky plagioclase (42%) up to 300 µm in length and minor embayed olivine (5%). Interstitial silica is common (7%). Randomly distributed laths of ilmenite (5%) up to 200 µm long, and rounded chromite (<1%) are also present. Sample 155_5A (1.3 x 1.2 mm, Fig. 1) is similar in texture and mineralogy, with a sub-ophitic texture consisting of large, zoned pyroxene (55%) and blocky intrafasciculate plagioclase ~300 µm in length (37%). Olivine (5%) is ~150 µm in diameter, rounded and embayed. Interstitial silica is common (7%). Occasional minor sulfides are associated with ilmenite.

Sample 155_9A (1.8 x 1.6 mm) is porphyritic and friable with large embayed, subhedral olivine phenocrysts (8% by mode) up to 300 µm in diameter and zoned pyroxene crystals (44% by mode including groundmass) up to 200 µm in size, set in a fine-grained groundmass of pyroxene, plagioclase, silica and ilmenite (Fig. 2). Occasional skeletal chromite grains (0.5%) are enclosed or partially enclosed in olivine. Acicular ilmenite laths 30 to 150 µm in length cross-cut the matrix but not the phenocrysts.

Sample 155_11A (1.3 x 0.9 mm) is variolitic and exhibits two distinct textures (Fig. 2). The sample contains anhedral silica (~200 µm in size, 9%), and Fe-rich pyroxene grains up to ~400 µm in size (43%) which are cross-cut by laths of ilmenite up to 600 µm long (4%). Plagioclase laths (43%) up to 600 µm in length (43%) are often enclosed by less Fe-rich pyroxene where they exhibit a branching, plumose texture, with intergrowths of plagioclase and pyroxene.

Sample 155_12A (1.4 x 1.1 mm) is sub-ophitic (Fig. 2), with highly zoned and rounded pyroxene (60%), up to 450 µm in diameter, plagioclase laths (31%) up to 600 µm long and elongate, bladed, ilmenite laths ~150 µm in length (4%). Skeletal silica crystals have conchoidal fractures, and account for 5% of the sample. Olivine is absent.

Three samples would be grouped as textural Type 2 under the scheme of Snape et al. (2014). Samples 155_2A and 155_6A have porphyritic textures and likely represent two parts of the same chip that broke in transit from JSC to London. Sample 155_2A (1.5 x 1.1 mm) consists of subhedral pyroxene (54%) and rounded olivine (12%) up to 300 µm in diameter (Fig. 1). Pyroxene crystals partially enclose blocky, skeletal plagioclase (31%). Ilmenite crystals (< 250 µm, 3%) are rounded to subhedral. Spinels are zoned from chromite cores to ulvöspinel rims. Minor Fe-Ni are accessory minerals. Sample 155_6A (1.5 x 1.4 mm) consists of zoned pyroxene crystals (57 %) up to 300 µm in size, sub-ophitically enclosing smaller plagioclase laths (30%) which are flow-aligned in places (Fig. 1). Fractured, glomerophyric phenocrysts of olivine up to 400 µm in size (6%) are confined to one area of the sample, and exhibit overgrowths of pyroxene. Accessory phases include interstitial silica (5 %), minor sub-micron Fe-Ni metal and phosphates (<15 µm).

Sample 155_10A (1.9 x 1.3 mm, Fig. 2) has a sub-ophitic texture dominated by zoned pyroxene (62%) ~300 to 350 µm in size, together with rounded, partially resorbed olivine (13%) ~300 µm in size, and branching 100 to 300 µm laths of plagioclase (19%). Ilmenite is minor (2%), ~150 µm in length, blocky in texture and intergrown with plagioclase in places. Minor chromite (2%) is zoned and anhedral. Fe-Ni grains and silica are present in the mesostasis.

Sample 155_1A (1.8 x 1.0 mm) is a coarse-grained fragment (Fig. 1) consisting mostly of pyroxene (93%) ~ 400 µm in size, which is unzoned, making it distinct from other samples (Figs. 1 and 2). Pyroxene poikilitically encloses smaller rounded olivine (2% by mode) and chromite / ulvöspinel grains (1% by mode, ~150 µm in size) together with traces of Fe-Ni metal. Minor interstitial plagioclase is also present (3%). The coarse-grained nature and small size of this sample suggest that it is not representative of the parent rock from which it was derived. Using the scheme of Snape et al. (2014), this sample would be textural Type 3.

Sample 155_8A (1.4 x 0.8 mm) is a textural Type 4 (Snape et al., 2014) and exhibits a microgabbroic texture (Fig. 2) with grain sizes up to 400 µm, consisting of subhedral olivine (14%) and pyroxene (68%), together with masses of coarse plagioclase (22%). Ulvöspinel crystals (1%) are completely enclosed within both pyroxene and feldspar.

Sample 155_7A (1.3 x 1.0 mm) does not easily fit the textural classification scheme of Snape et al. (2014), although it is closest to two of the Type 4 samples in that study. It is comparatively rich in ilmenite (6%), which occurs as coarse masses up to 300 µm in size, as does plagioclase (22%) in sizes up to 400 × 200 µm (Fig. 2). Olivine (2% of the sample; 100 µm in size) is enclosed within pyroxene cores. Pyroxene crystals (68%) are ~ 300 µm in size. Troilite (FeS) and ulvöspinel (1%) are minor phases, and there are irregular patches of Si- and K-rich glass which contain sub-micron grains of Fe-Ni metal. The sample is generally granular in texture with irregular, patchy zoning, which may indicate some degree of shock processing.

3.2 Bulk Compositions

Bulk compositions of the samples (Table 2) indicate that they are all low-Ti (1-6 wt% TiO_2) basalts. Al_2O_3 contents are highly variable (5.6 to 12.3 wt%, excluding 155_1A which has only 2.3 wt% Al_2O_3). SiO_2 contents show a narrow range (43.9 to 46.9 wt%) with the exception of 155_1A (51.5 wt% SiO_2), although this sample is coarse-grained and likely not representative. Generally, bulk TiO_2 and Al_2O_3 contents increase with decreasing bulk Mg# (Table 2).

3.3 Mineral Chemistry

3.3.1 Pyroxene

Pyroxene grains in the chips show a wide range of compositions ($En_{0\text{-}67}Fs_{20\text{-}90}Wo_{7\text{-}40}$; Fig. 3, Appendix S1). Most samples exhibit compositional zoning with Mg-rich pigeonite or augite cores mantled by augite. Pyroxene compositions change from the cores towards the rims, forming progressively more Fe-rich rims, with extreme Fe-enrichment in some samples (e.g., samples 155_2A, 3A, 4A, 5A, 6A, 11A and 12A).

Pyroxene in 155_1A is almost entirely pigeonite ($En_{53\text{-}65}Fs_{26\text{-}35}Wo_{7\text{-}12}$) which exhibits weaker zoning than other samples. There is only one augite crystal ($En_{42\text{-}50}Fs_{21\text{-}26}Wo_{28\text{-}29}$). Mg# for all pyroxenes in this sample are high (56 to 71) and no Fe-rich grains or rims were detected (Fig. 3).

While 155_1A and 155_8A show the least Fe-enrichment in pyroxene compositions, pyroxenes in 155_7A also show a narrower compositional range than some other samples, with a relatively restricted range of Mg# (32 to 67) but a wide range of Wo contents ($En_{24\text{-}56}Fs_{20\text{-}54}Wo_{10\text{-}40}$). Sample 155_11A contains pyroxene that is compositionally distinct from other samples. Although the pyroxene is zoned ($En_{0\text{-}43}Fs_{40\text{-}85}Wo_{12\text{-}33}$), no Mg-rich pyroxene is present (Mg# <50 in all measurements), attesting to the evolved nature of the melt from which it crystallised.

Sample 155_12A displays the widest range of pyroxene compositions of the studied samples ($En_{2\text{-}65}Fs_{23\text{-}83}Wo_{7\text{-}37}$), and some of the most Mg-rich cores (max. Mg# 72), comparable with those in 155_1A (Mg# 56 to 71).

Trace element abundances were measured in pyroxene phases from the 12 samples (Appendix S2). Most samples show a range of compositions, which vary in accordance with major element composition: pigeonite cores have lower concentrations of trace elements, whilst Wo-richer augite mantles and Fe-rich rims have higher concentrations, as expected from crystals precipitating from a fractionating melt. The rare earth elements (REE) have lower chondrite normalised (subscript 'cn'; CI chondrite values from Anders and Grevesse, 1989) light-REE (LREE) relative to heavy-REE (HREE) with $(La/Lu)_{cn}$ ranging from 0.02 to 0.84 (Appendix S2). The slope from Ce to Sm becomes less steep with increasing Ca in agreement with the trend

noted by Shearer et al. (1988). Pyroxene also show negative Eu-anomalies with Eu/Eu^{*} ($2Eu_{cn}/[Sm_{cn} + Gd_{cn}]$) giving values from 0.09 to 0.78.

Pigeonite REE concentrations in 155_1A are the lowest of the studied 12023 basalt chips (Appendix S2), while sample 155_12A has the widest range of pyroxene trace element concentrations. Samples 155_6A and 155_11A show similar trends in pyroxene to the other samples but with particularly high REE in the Fe-rich rim compositions (up to 100× CI chondritic). Although cores in 155_7A have lower concentrations of REE, there is no significant difference between compositions of the cores and rims in this sample.

3.3.2 Plagioclase

Plagioclase is abundant in all samples (Appendix S1), with the exception of 155_1A where it is a minor phase. Most samples contain anorthitic plagioclase (An_{83-94}, Appendix S3), with little compositional variation, although variation of An with plagioclase Mg# highlights some important differences in crystallisation trends between the samples (Fig. 4). Sample 155_7A shows a wider range of compositions ($An_{76-93}Or_{0-4}$), elevated Na_2O and K_2O and a different crystallisation trend to other samples (Fig. 4). The most Ca-rich plagioclase crystals occur in 155_8A (An_{87-94}). Plagioclase in 155_1A is relatively Ca-poor ($An_{83}Or_1$) in comparison with the other samples.

Trace element concentrations were also measured in plagioclase (Appendix S1) where crystal size permitted analysis (Appendix S4). All profiles show positive Eu-anomalies. Sample 155_1A has the highest concentrations of Eu (4.37 ppm) and Sr (593 ppm) in plagioclase, but has lower concentrations of other REE's than the other samples.

3.3.3 Olivine

Major and trace element analyses of olivine are given in Appendix S1. Olivine Fo (atomic Mg/(Mg+Fe)x100) contents range from 34 to 74 (Fig. 5), with the widest range and the lowest forsterite contents in 155_7A (Fo_{34-55}). Sample 155_8A also exhibits low forsterite contents (Fo_{48-57}) but is still within a typical range for mare basalts of Fo_{30-80} (Papike et al., 1998). No extreme fayalitic compositions were observed in any of the 12023 basalt regolith chips. Trace elements showed a range of concentrations (Fig. 5). Olivine Ti/V ratios are similar for most samples (2 to 3), although much higher values are seen for the coarser grained samples 155_1A (4.1 to 8.3), 7A (9.0) and 8A (13.1 to 15.5), which also have lower Fo contents. Samples 155_7A and 8A also have higher Mn abundances than other samples. Sample 155_1A does not have high Mn, but has low contents of Ni (40.8 – 54.5 ppm, Appendix S1), in common with 155_7A and 155_8A (36.8 – 72.7 ppm).

3.3.4 Chromite and Ulvöspinel

Samples 155_4A, 9A and 10A contain chromite only, while 155_7A and 8A contain only ulvöspinel. Chromite and ulvöspinel occur as separate grains in sample 155_1A (Table 1), whereas in samples 155_2A and 6A they are zoned from chromite cores to ulvöspinel rims ($2Ti_{12-97}Al_{2-20}Cr_{0.4-69}$; Appendix S1) and follow a typical mare basalt fractionation trend (Appendix S5). There is a compositional gap between chromite and ulvöspinel, which has been interpreted as the result of partial resorption of Ti-rich chromite during slow cooling (Arai et al., 1996).

3.3.5 Other phases

All samples with the exception of 155_1A contain ilmenite with modal percentages ranging from <1% (155_8A) to 7% (155_9A). Major element analyses are listed in Appendix S1. Silica phases were not seen in 12023,155_1A, 8A or 12A. All other samples contain silica with modal percentages between <1% (155_8A) and 9% (155_11A, Table 1) and analyses are given in Appendix S1. In addition, samples 155_5A, 7A and 10A contained patches of Si- and K-rich glass (Appendix S1: 3.5 to 7.7 wt% K_2O in 155_7A, 5.9 to 6.4 wt% K_2O in 155_5A and 6.7 to 7.0 wt% K_2O in 155_10A). This phase contains Fe-Ni inclusions in samples 155_7A and 155_10A that are too small to resolve with the EMPA.

4 Discussion

4.1 Evaluation of the representativeness of samples through estimation of parental melt composition.

It has been demonstrated by many authors (e.g., Roeder and Emslie, 1970; Papike et al., 1976; Dungan and Brown, 1977; Joy et al., 2008) that it is possible to model equilibrium parent melt Mg# from olivine compositions in lunar samples and to predict equilibrium liquidus olivine Mg# from the bulk compositions using the following equations (Roeder and Emslie, 1970; Niu et al., 2002):

$$\text{Melt Mg\#} = 1/ ([1/\text{Olivine Fo} - 1]/K_d + 1) \quad (1)$$

$$\text{Olivine Fo} = 1/ (K_d \times [1/ \text{Melt Mg\#} - 1] + 1) \quad (2)$$

where K_d is the distribution coefficient for partitioning of Fe and Mg between olivine and co-existing melt. A K_d of 0.33 applicable for lunar basaltic melts (Grove and Vaniman, 1978; Longhi et al., 1978) is assumed. For most samples, these equations recreate the bulk rock Mg# and olivine Mg# with reasonable accuracy (Table 3), which suggests that olivine was in equilibrium with the melt (as represented by the bulk rock composition: Table 2). However, several samples do not reflect this relationship: Samples 155_1A, 7A, 8A and 10A do not contain olivine with the high Mg# predicted by their bulk composition Mg#. Samples 155_1A and 8A are both coarse-grained and, together with 155_10A, show signs of mineral composition chemical equilibration (Fig. 3). Sample 155_7A is also relatively coarse-grained and its patchy zoning indicates that shock processing may have affected the mineral chemistry. With the exception of these samples, and those that lack olivine, results suggest that the measured bulk compositions of the samples (Table 2) are representative of the parent melts for 155_2A, 4A, 5A, 6A and 9A, despite the small sample sizes, and demonstrate that our method of determining the bulk composition yields reliable results.

Previous studies (Arai et al., 1996, 1999, 2010) have shown that the bulk rock TiO_2 can also be estimated from pyroxene compositions by plotting pyroxene Fe# (atomic Fe/[Fe + Mg] x 100) vs. Ti# (atomic Ti/[Ti +Cr] x 100): Appendix S6). This is useful for coarser grained basalt types which may not represent a magma composition and is important as the bulk TiO_2 content is the major distinguishing factor for different lunar basalt types. Using the method described by Arai et al. (1996), at pyroxene Fe# 50 the corresponding range of Ti# in all the chips where olivine is present is 80 – 85, giving a reconstructed bulk TiO_2 value of approximately 4.0 – 4.5 %. These values are narrower than those measured from the bulk compositions (between 3 – 6 wt% (Table 2)), with the exception of 155_1A, 8A and 10A, which are unrepresentative). Therefore, this method provides additional evidence that all the samples in this study, including the coarse-grained samples, are low-Ti basalt types.

4.2 Comparison with other samples from the Apollo 12 landing site.

The studied samples exhibit a variety of textures and compositions. Comparisons with other known Apollo 12 basalts enable us to establish which samples represent local lithologies and which require separate parent magmas or may represent non-local lithologies.

Fagan et al. (2013) and Snape et al. (2014) used trace elements in olivine in order to distinguish between the different Apollo 12 basalt groups, and we apply these criteria to the olivine-bearing samples in this study (Fig. 5c). However, Sc contents in olivine show a narrow range, making it difficult to distinguish between pigeonite and olivine basalts using this method. Olivine in 12023,155_2A, 6A, 4A, 5A and 10A all have low Ti/V ratios (1.99 to 3.17), but a narrow range of Sc contents (9.6 to 14.8 ppm) possibly indicating that these samples are sourced from either an olivine or pigeonite basalt lava flow. Samples 12023,155_1A, 7A and 8A all have higher Ti/V ratios because of the low V contents in their olivine. However, 155_1A and 8A contain few ilmenite crystals and are, thus, unlikely to be ilmenite basalts. Equilibration temperatures control the amount of V in olivine (De Hoog et al., 2010), which will have affected the chemistry in these coarser-grained more slowly-cooled samples. Pyroxene REE concentrations are similar to those in other Apollo 12 basalts but do not clearly delineate between the sample groups.

4.2.1. Probable local lithologies

Samples 155_2A, 6A, 8A, 9A and 10A are all similar to olivine basalts from the Apollo 12 site. Samples 155_2A and 155_6A have similar mineral chemistries to the porphyritic olivine basalt 12004 (Brett et al., 1971; Walter et al., 1971). Sample 155_8A is a coarser-grained microgabbroic sample. It has the highest An and lowest Fe and Mg contents in plagioclase of the samples studied, typical of slow cooling in basalts (Longhi et al., 1976). Its Ti/V ratios in olivine suggest that it is comparable with ilmenite basalts (Fig. 5). However, in this case the

low V contents are interpreted as an equilibration effect together with partitioning into early crystallising spinel. It shows some similarities to olivine basalt/microgabbro 12035, which has equilibrated Fe-rich olivine and re-equilibrated spinel (Reid, 1971). Sample 155_9A is similar to Apollo 12 samples 12008, 12045 and 12022. Its Fe/Mg ratio is particularly similar to 12008 and 12022 (~3% difference between Mg#s for these samples and 155_9A). Sample 155_10A is coarse-grained and its bulk chemistry is not representative. However, the similarities in olivine chemistry between this sample and 155_2A and 155_6A together indicate that it is also an olivine basalt.

Sample 155_3A is likely to represent an ilmenite basalt fragment on the basis of its bulk Mg# and TiO_2 contents, which are similar to Apollo 12 basalts 12047, 12051 and 12039. Pyroxene compositions in 12051 are comparable, with extreme Fe-enrichment at the rims (Brown et al., 1971; Keil et al., 1971) and absence of olivine (McGee et al., 1977).

Sample 155_12A appears similar in terms of its texture, bulk chemistry, modal mineralogy and mineral chemistry to many pigeonite basalts from the Apollo 12 site. This sample is particularly similar to the Apollo 12 pigeonite basalt 12021, which has a similar wide range of pyroxene compositions including Mg-rich core compositions (Dence et al., 1971; Weill et al., 1971).

4.2.2 Distinct or non-local lithologies

Sample 12023,155_1A is coarse-grained and may be unrepresentative of its parent rock. However, its mineral chemistries also show marked differences compared to other samples in this study, with different mineral compositions in olivine (Fig. 5) and chromite to ulvöspinel crystallisation trends (Appendix S5). Plagioclase are less anorthitic in 155_1A when plotted against Mg# in olivine (Appendix S7). This sample exhibits a similar range of olivine and pyroxene compositions to 12005 (Dungan and Brown, 1977), and has a similar Ti/V ratio in olivine (4.5 in 12005 (Fagan et al., 2013); and 4.1 to 8.3 in olivine from 155_1A). Although 12005 is classified as an ilmenite basalt, it is also atypical and deemed unrepresentative of the ilmenite basalt parent lava flow (Neal et al., 1994a, 1994b).

Samples 155_4A and 155_5A are similar to feldspathic basalt 12038. Both have high bulk Al_2O_3 contents (11.9 and 12.3 wt% respectively) and low-Ti contents (<4 wt% TiO_2). Sample 155_5A has the lowest bulk FeO contents of all samples studied (17.7 wt %), although it is acknowledged that the small size of these samples means that reliance on bulk chemistry alone is not conclusive. Plagioclase and pyroxene compositions span a similar range to 12038 with similar concentrations of REE in pyroxene. Given that other soil fragments from the Apollo 12 site have recently been tentatively identified as feldspathic basalts (12032,366_03 and 12023,143_03 (Korotev et al., 2011); and 12003,314 (Snape et al.,2014)), it is possible that these may be additional examples from this lithological group. Sample 12038 was collected from a different sampling station to 12023. The presence of feldspathic basalts at different sampling localities increases the likelihood that feldspathic basalts represent a separate flow at the Apollo 12 site and are less likely to be material introduced by impacts, as suggested by Neal et al. (1994).

Sample 155_7A is too coarse-grained to be representative in terms of its mineralogy and bulk chemistry, but it would be classified as an ilmenite basalt on the basis of its Ti/V ratio of olivine (after Fagan et al., 2013; Fig. 5). However, it has distinctly different plagioclase chemistry and crystallisation trends (Fig. 4) from the other samples studied, as well as a wider range of Mg# in olivine compared with other Apollo 12 basalts (Fig. 5). It shows more similarities to Apollo 14 high-Al basalts in terms of plagioclase An# (77-93 for Group B high-Al basalts: Neal and Kramer, 2006; Hui et al., 2011) and Fo contents in olivine (Fo_{39-78}: Dickinson et al., 1985; Hagerty et al., 2005). Olivine chemistry shows that Ti/V ratios and Sc contents are also similar in Apollo 14 high-Al basalts (Fagan et al., 2013) as are compatible elements Ni and Co (Hagerty et al., 2005). This sample may, therefore, represent a lithology more like the Apollo 14 basalts than Apollo 12 basalts.

Sample 155_11A has a lower bulk Mg# (21.6) than all other Apollo 12 basalts and its pyroxene grains are all Fe-rich (Fig. 3). Although care needs to be taken regarding the representativeness of small samples, 155_11A is a fine-grained variolitic sample with highly zoned pyroxene and, as such, is more likely to be representative of its parent lava flow in terms of its bulk composition than 155_1A. Despite these differences, this sample shows similar crystallisation trends and mineral chemistries to the Fe-enriched late-stage minerals in other Apollo 12 samples. Therefore, we conclude that sample 155_11A is likely to be from a more highly fractionated Apollo 12 basaltic melt, rather than being exotic to the Apollo 12 site.

5 Conclusions and further work

We have presented a geochemical and petrological analysis of 12 coarse fines from the lunar soil sample 12023. These samples show a wide range of textures, mineralogies and chemistries, despite being collected from one site. Problems of unrepresentativeness of small samples are acknowledged. Some of these have been partially addressed by calculating the equilibrium Mg# from the olivine Mg# and vice versa. Where the sample is fine-grained and the bulk Mg# can be calculated with reasonable accuracy then the sample may be deemed representative and classified according to the bulk chemical properties, backed up by mineral chemistry. Where this is not possible, we have shown that a combination of major, minor and trace element analyses may be used to identify basaltic fragments derived from different sources.

These samples have all been shown to be low-Ti basalts, many of which have bulk chemical compositions and mineral chemistries consistent with the previously identified olivine, pigeonite or ilmenite Apollo 12 basalt lithological groups. There are five exceptions, as follows:

(i) Sample 12023,155_1A has mineral and trace element chemistries which suggest that it is distinct from other Apollo 12 samples and may require a separate parent magma.

(ii) Sample 155_7A is identified as a potential exotic fragment that has greater similarities to Apollo 14 basalts than to those at the Apollo 12 site.

(iii) Samples 12023,155_4A and 5A have chemical similarities to feldspathic basalt 12038. These samples may therefore represent additions to the feldspathic basalt group, indicating that feldspathic basalts may represent a local lava flow in accordance with Snape et al. (2014), rather than material introduced by impacts from a more distant location as suggested by Neal et al. (1994a).

(iv) Sample 155_11A is compositionally anomalous compared to Apollo 12 basalts and basaltic fragments, with an exceptionally low bulk Mg# of 21.6 and Fe-rich mineral chemistries. This sample may represent a highly fractionated Fe-rich Apollo 12 basalt, not currently represented by other Apollo 12 samples.

Therefore, even bearing in mind the possibly unrepresentative nature of small samples, at least one, and possibly as many as four, separate parent magmas appear to be required, in addition to the previously identified olivine, ilmenite and pigeonite basalt magmas, in order to account for the chemical and textural diversity found in this study. Ultimately, results from radiometric dating will be needed to determine if samples may represent younger, exotic material transferred from other areas.

Acknowledgements

We are grateful to CAPTEM for sample allocation and to the staff of the Lunar Sample Curation Facility at NASA JSC for their expert assistance in the selection and processing of these samples. We thank Dr. Andy Beard at Birkbeck for his assistance with electron microprobe techniques, and Dr. Martin Rittner, Birkbeck, for his assistance with using the LA-ICP-MS. We are also grateful to Dr. Adrian Jones, UCL, for useful petrology discussions. We thank Drs. Randy Korotev, Akira Yamaguchi and Tomoko Arai, and an anonymous reviewer, for providing thoughtful advice on previous versions of the manuscript. Birkbeck College and The Leverhulme Trust (grant 2011-569 to KHJ) are thanked for financial support.

References

Anders, E., and Grevesse, N. (1989). Abundances of the elements: Meteoritic and solar. Geochimica et Cosmochimica Acta 53: 97-214.

Anderson, A.T. Jr., and Smith, J.V. (1971). Nature, occurrence and exotic origin of “gray mottled” (Luny Rock) basalts in Apollo 12 soils and breccias. Proceedings, Lunar and Planetary Science Conference, vol.2, p.431.

Arai, T., Takeda, H. and Warren, P.H. (1996). Four lunar meteorites: Crystallization trends of pyroxenes and spinels. Meteoritics & Planetary Science 31: 877-892.

Arai, T., and Warren, P.H. (1999) Lunar Meteorite Queen Alexandra Range 94281: Glass compositions and other evidence for launch pairing with Yamato 793274. Meteoritics & Planetary Science 34: 209-234.

Arai, T., Takeda, H., and Miyamoto M. (2006). Spinel crystallisation in the ancient lunar mare basalt Asuka 881757 as a petrogenetic indicator. Antarctic Meteorite Research 19, 1-19.

Arai, T., Hawke, B.R,, Giguere, T.A., Misawa, K., Miyamoto, M., Kojima, H. (2010). Antarctic lunar meteorites Yamato-793169, Asuka-881757, MIL 05035, and MET 01210 (YAMM): Launch pairing and possible cryptomare origin. Geochimica et Cosmochimica Acta 74: 2231-2248.

Baldridge, W.S., Beaty, D.W., Hill, S.M.R. and Albee, A.L. (1979). The petrology of the Apollo 12 pigeonite basalt suite. Proceedings, 10th Lunar and Planetary Science Conference. pp. 141-179.

Barnes, S.J. (1986). The effect of trapped liquid crystallization on cumulus mineral compositions in layered intrusions. Contributions to Mineralogy and Petrology 93: 524-531.

Beaty, D.W., Hill, S.M.R., Albee,A.L., and Baldridge, W.S. (1979). Apollo 12 feldspathic basalts 12031, 12038 and 12072: Petrology, comparison and interpretations. Proceedings, 10th Lunar and Planetary Science Conference. pp. 115-139.

Becker R.H. and Clayton R.N. (1978) Nitrogen isotope systematics of two Apollo 12 soils. Proceedings. 9th Lunar Planetary Science Conference: 1619-1628.

Bence, A.E., Papike, J.J., and Prewitt, C.T. (1970). Apollo 12 clinopyroxenes: Chemical trends. Earth and Planetary Science Letters 8: 393.

Borg, L.E., Gaffney, A.M., Shearer, C.K., DePaolo, D.J., Hutcheon, I.D., Owens, T.L., Ramon, E., Brennecka, G. (2009). Mechanisms for Incompatible-element Enrichment on the Moon deduced from Lunar Basaltic Meteorite Northwest Africa 032. Geochimica et Cosmochimica Acta 73: 3963-3980.

Brett, R., Butler, P.J., Meyer, C., Reid, A.M., Takeda, H., and Williams, R. (1971). Apollo 12 igneous rocks 12004, 12008, 12009 and 12022: A mineralogical and petrological study. Proceedings, Lunar and Planetary Science Conference, vol.2, pp.301-317.

Brown, G.M., Emeleus, C.H., Holland, J.G., Peckett, A. and Phillips, R. (1971). Picrite basalts, ferrobasalts, feldspathic norites, and rhyolites in a strongly fractionated lunar crust. Proceedings, Lunar and Planetary Science Conference, vol. 2, p.583.

Butler, P. Jr. (1972). Compositional characteristics of olivines from Apollo 12 samples. Geochimica et Cosmochimica Acta 36: 773-785.

Cameron, E.N. (1971). Opaque minerals in certain lunar rocks from Apollo 12. Proceedings, 2nd Lunar and Planetary Science Conference:193 - 206.

Champness, P.E., Dunham, A.C., Gibb, F.G.F., Giles, H.N., MacKenzie, W.S., Stumpfl, E.F., Zussman, J. (1971). Mineralogy and petrology of some Apollo 12 samples. Proceedings, 2nd Lunar and Planetary Science Conference: 359 - 376.

Crawford M. L. 1973. Crystallization of plagioclase in mare basalts. Proceedings, 4th Lunar and Planetary Science Conference. p. 705.

Crawford, I. A., Fagents, S.A., and Joy, K.H. (2007) Full Moon exploration. Astronomy and Geophysics 48: Issue 3, 18 – 21.

Cuttitta F., Rose H.J.Jr., Annell C.S., Carron M.K., Christian R.P., Dwornik E.J., Greenland L.P., Helz A.P., and Ligon D.T. Jr. (1971) Elemental composition of some Apollo 12 lunar rocks and soils. Proceedings, Lunar and Planetary Science Conference, vol.2, pp. 1217-1229.

De Hoog, J.C.M., Gall, L., and Cornell, D.H. (2010). Trace-element geochemistry of mantle olivine and application to mantle petrogenesis and geothermobarometry. Chemical Geology 270: 196-215.

Dence, M.R., Douglas, J.A.V., Plant, A.G., and Traill, R.J. (1971). Proceedings, Lunar and Planetary Science Conference, vol.2, p.285.

Dickinson T., Taylor G. J., Keil K. Schmitt R. A., Hughes S. S., and Smith M. R. (1985). Apollo 14 aluminous mare basalts and their possible relationship to KREEP. Proceedings, 15th Lunar and Planetary Science Conference. pp. 365 - 374

Dickinson T., Taylor G.J., Keil K., and Bild R.W. (1989) Germanium abundances in lunar basalts: Evidence of mantle metasomatism. Proceedings, 19th Lunar and Planetary Science Conference. pp. 189-198.

Drake, M.J., McCallum, I.S., McKay, G.A., and Weill, D.F. (1970). Mineralogy and petrology of Apollo 12 sample No. 12013: A progress report. Earth and Planetary Science Letters 9: 103-123.

Dungan, M.A., and Brown, R.W. (1977). The petrology of the Apollo 12 ilmenite basalt suite. Proceedings, 8th Lunar and Planetary Science Conference. pp. 1339-1381.

El Goresy, A., Ramdohr, P., and Taylor, L.A. (1971). The opaque minerals in the lunar rocks from Oceanus Procellarum. Proceedings, Lunar and Planetary Science Conference, vol.2, p.219.

Fagan, A.L., Neal, C.R., Simonetti, A., Donohue, P.H., and O'Sullivan, K.M. (2013). Distinguishing between Apollo 14 impact melt and pristine mare basalt samples by geochemical and textural analyses of olivine. Geochimica et Cosmochimica Acta 106: 429 – 445

Gibb, F.G.F., Stumpfl, E.F., and Zussman, J. (1970). Opaque minerals in an Apollo 12 rock. Earth and Planetary Science Letters 9: 217-224.

Grove, T.L., and Vaniman, D.T. (1978). Experimental petrology of very low Ti/VLT/basalts. Mare Crisium: The view from Luna, 24, pp.445-471. Pergamon Press Inc., New York

Hagerty, J.J., Shearer, C.K., and Papike, J.J. (2005). Petrogenesis of the Apollo 14 high-alumina basalts: Implications from ion microprobe analyses. Geochimica et Cosmochimica Acta 69: 5831 – 5845.

Haggerty, S.E. and Meyer, H.O.A. (1970). Apollo 12: Opaque oxides. Earth and Planetary Science Letters 9: 379-387.

Hiesinger, H., Head, J.W. III, Wolf, U., Jaumann R., and Neukam, G. (2003). Ages and stratigraphy of mare basalts in Oceanus Procellarum, Mare Nubium, Mare Cognitum and Mare Insularum. Journal of Geophysical Research 108:5065. doi: 10.1029/2002JE001985

Hiesinger, H., Head III, J.W., Wolf, U., Jaumann, R., Neukum, G. (2010). Ages and stratigraphy of lunar mare basalts in Mare Frigoris and other nearside maria based on crater size-frequency distribution measurements. Journal of Geophysical Research 115: E03003. doi: 10.1029/2009JE003380

Hollister, L.S., Trzcienski, Jr., W.E., Hargreaves, R.B., and Kulick, C.G. (1971). Petrogenetic significance of pyroxenes in two Apollo 12 samples. Proceedings, Lunar and Planetary Science Conference, vol.2, p.529.

Hui, H., Oshrin, J.G., and Neal, C.R. (2011). Investigation into the petrogenesis of Apollo 14 high-Al basaltic melts through crystal stratigraphy of plagioclase. Geochimica et Cosmochimica Acta 75: 6439 – 6460.

James, O.B., and Wright, T.L. (1972). Apollo 11 and 12 mare basalts and gabbros: Classification, compositional variations, and possible petrogenetic relations. Geological Society of America bulletin, 83, 2357-2382.

Jones, J.H. (1995). Experimental trace element partitioning rock physics and relationships. In A Handbook of Physical Constants, American Geophysical Union, p.p. 74-104.

Joy, K.H., Crawford, I.A., Downes, H., Russell, S.S., and Kearsley, A.T. (2006). A petrological, mineralogical, and chemical analysis of the lunar mare basalt meteorite La Paz Icefield 02205, 02224 and 02206. Meteoritics & Planetary Science 41: 7, 1003-1025.

Joy, K.H., Crawford, I.A., Anand, M., Greenwood, R.C., Franchi, I.A., and Russell, S.S. (2008). The petrology and geochemistry of Miller Range 05035: A new lunar gabbroic meteorite. Geochimica et Cosmochimica Acta 72: 3822-3844

Joy, K.H., Crawford, I.A., Russell, S.S., and Kearsley, A.T. (2010). Lunar meteorite regolith breccias: An in situ study of impact melt composition using LA-ICP-MS with implications for the composition of the lunar crust. Meteoritics & Planetary Science 45: 917-946

Joy K. H., Ross D. K., Zolensky M. E., and Kring D. A. (2011). Reconnaissance Element Mapping of Lunar Regolith Breccias (abstract #2007). *2011 Annual Meeting of the Lunar Exploration Analysis Group.*

Keil, K., Prinz, M. and Bunch, T.E. (1971). Mineralogy, petrology and chemistry of some Apollo 12 samples. Proceedings, Lunar and Planetary Science Conference, vol.2, p. 319.

Korotev, R.L., Joliff, B.L., Zeigler, R.A., Seddio, S.M., and Haskin, L.A. (2011). Apollo 12 Revisited. Geochimica et Cosmochimica Acta 75: 1540-1573

Kushiro, I., and Haramura, H. (1971). Major element variation and possible source materials of Apollo 12 crystalline rocks. Science 171: 1235-1237.

Levine J., Becker T. A., Muller R. A., and Renne P. R. (2005) $^{40}Ar/^{39}Ar$ dating of Apollo 12 impact spherules. Geophysical Research Letters 32(15): L15201.

Li, L. and Mustard, J. F. (2005). On lateral mixing efficiency of lunar regolith. Journal of Geophysical Research 110: E11002. doi: 10.1029/2004JE002295

LSPET (Lunar Sample Preliminary Examination Team), (1970). Preliminary examination of lunar samples from Apollo 12. Science 167: 1325-1339

Lunatic Asylum (1970). Mineralogic and isotopic investigations on lunar rock 12013. Earth and Planetary Science Letters 9: 137-163.

Longhi, J., Walker, D., and Hays, J.F. (1976). Fe and Mg in plagioclase. Proceedings, 7th Lunar and Planetary Science Conference. pp 1281-1300.

Longhi , J., Walker, D., and Hays, J.F. (1978). The distribution of Fe and Mg between olivine and lunar basaltic liquids. Geochimica et Cosmochimica Acta 42: 1545-1558.

Maxwell J.A. and Wiik H.B. (1971). Chemical compositions of Apollo 12 lunar samples 12004, 12033, 12051, 12052, and 12065. Earth and Planetary Science Letters 10: 285-288.

McGee, P.E., Warner, J.L., and Simonds, C.H. (1977). Introduction to the Apollo collections. Part 1: Lunar Igneous Rocks. Curators Office, JSC.

Meyer, C. (2010). 12005 Ilmenite basalt. Lunar Sample Compendium. http://curator.jsc.nasa.gov/lunar/lsc/12005.pdf

Morrisson G.H., Gerard J.T., Potter N.M., Gangadharam E.V., Rothenberg A.M., and Burdo R.A. (1971) Elemental abundances of lunar soil and rocks from Apollo 12. Proceedings, 2nd Lunar and Planetary Science Conference: 1169-1185.

Neal, C.R., and Taylor, L.A. (1992). Petrogenesis of mare basalts: A record of lunar volcanism. Geochimica et Cosmochimica Acta 56: 2177-2211.

Neal C.R., Hacker M.D., Snyder G.A., Taylor L.A., Liu Y-G., and Schmitt R.A. (1994a). Basalt generation at the Apollo 12 site, Part 1: New data, classification, and re-evaluation. Meteoritics 29: 334-348.

Neal C.R., Hacker M.D., Snyder G.A., Taylor L.A., Liu Y-G., and Schmitt R.A. (1994b). Basalt generation at the Apollo 12 site, Part 2: Source heterogeneity, multiple melts, and crustal contamination. Meteoritics 29: 349-361.

Neal, C.R., and Kramer, G.Y. (2006). The petrogenesis of the Apollo 14 high-Al mare basalts. American Mineralogist 91**:** 1521**–**1535**.**

Newton, R.C., Anderson, A.T., and Smith, J.V. (1971). Accumulation of olivine in rock 12040 and other basaltic fragments in the light of analysis and syntheses. Proceedings, Lunar and Planetary Science Conference, vol.2, p.575.

Niu, Y.L., Gilmore, T., Mackie, S., Greig, A., and Bach, W. (2002a). Mineral chemistry, whole-rock compositions and petrogenesis of ODP Leg 176 gabbros: data and discussion. In Natland J.H., Dick, H.J.B., Miler, D.J., Van Herzen, R.P. (Eds). Proceedings, Ocean Drilling Program: Science Results vol. 176, pp. 1-60.

National Research Council of the National Academies (NRC) (2007). The Scientific Context for Exploration of the Moon. The National Academies Press, Washington, D.C.

Nyquist L.E., Shih C.-Y., Wooden J.L., Bansal B.M., and Wiesmann H. (1979). The Sr and Nd isotopic record of Apollo 12 basalts: Implications for lunar geochemical evolution. Proceedings, 10th Lunar and Planetary Science Conference. pp 77-114.

Nyquist L.E., Wooden J.L., Shih C.-Y., Wiesmann H., and Bansal B.M. (1981). Isotopic and REE studies of lunar basalt 12038: implications for petrogenesis of aluminous mare basalts. Earth and Planetary Science Letters 55: 335-355.

Papike J.J., Bence, A.E., and Lindsley, D.H. (1974). Mare basalts from the Taurus-Littrow region of the Moon. Proceedings, 5th Lunar and Planetary Science Conference. pp 471-504

Papike, J.J., and Vaniman, D.T. (1978). Luna 24 ferrobasalts and the mare basalt suite: Comparative chemistry, mineralogy, and petrology. In Mare Crisium: The view from Luna 24 (J.J. Papike and R.B. Merrill, eds.), pp. 371 – 401. Pergamon, New York.

Papike, J.J., Hodges, F.N., Bence, A.E., Cameron, M., and Rhodes, J.M. (1976). Mare Basalts: Crystal Chemistry, mineralogy and petrology. Reviews of Geophysics Space Physics 14:475-540.

Papike, J., Taylor, L., and Simon, S. (1991). Lunar Minerals. In Heiken, G.H., Vaniman, D.T., French, B.M. (Eds). Lunar Sourcebook, Cambridge University Press pp.121-181.

Papike, J.J., Ryder G., and Shearer, C.K. (1998). Lunar Samples. Reviews in Mineralogy, 36, pp 5-1 – 5-234.

Pearce, N.J.G., Perkins, W.T., Westgate, J.A., Gorton, M.P., Jackson, S.E., Neal, C.R., and Chenery, S.P. (1997). A compilation of new and published major and trace element data for NIST SRM 610 and NIST SRM 612 glass reference materials. Geostandards Newsletter. Journal of Geostandards and Geoanalysis 21: 115-144.

Petro, N.E., and Pieters, C.M. (2007). Foreign Material in the lunar regolith: Lateral transport by post-basin cratering (abstract #2069). 38th Lunar & Planetary Science Conference. CD-ROM.

Reid, J.B. (1971). Apollo 12 spinels as petrogenetic indicators. Earth and Planetary Science Letters 10: 351-356.

Rhodes J.M., Blanchard D.P., Dungan M.A., Brannon J.C., and Rodgers K.V. (1977) Chemistry of Apollo 12 mare basalts: Magma types and fractionation processes. Proceedings, 8th Lunar and Planetary Science Conference. pp 1305-1338.

Roeder, P.L., and Emslie, R.F. (1970). Olivine-liquid equilibrium. Contributions to Mineralogy and Petrology 29:275.

Ryder G. and Schuraytz B. C. 2001. Chemical variation of the large Apollo 15 olivine-normative mare basalt rock samples. Journal of Geophysical Research 106:1435–1451.

Schnare, D.W., Day, J.M.D., Norman, M.D., Liu, Y., and Taylor, L.A. (2008). A laser-ablation ICP-MS study of Apollo 15 low-titanium olivine-normative and quartz-normative mare basalts. Geochimica et Cosmochimica Acta *72: 2556-2572.*

Shearer, C.K., Papike, J.J., Simon, S.B., and Shimizu, N. (1988). An ion microprobe study of the intra-crystalline behaviour of REE and selected trace elements in pyroxenes from mare basalts with different cooling and crystallisation histories; Preliminary results. 19th Lunar and Planetary Science Conference: 1071.

Shearer, C.K., and Papike, J.J. (1992). Relationship between Apollo 12 high-Ti red-picritic glass and high-Ti basaltic magmatism (abstract #1281). 23rd Lunar & Planetary Science Conference. CD-ROM.

Shearer C.K., and Papike J.J. (2005). Early crustal building processes on the Moon: Models for the petrogenesis of the magnesian suite. Geochimica et Cosmochimica Acta 69: 3445-3461.

Shearer, C.K., Hess, P.C., Wieczorek, M.A., Pritchard, M.E., Parmentier, E.M., Borg, L.E., Longhi, J., Elkins-Tanton, L.T., Neal, C.R., Antonenko, I., Canup, R.M., Halliday, A.N., Grove, T.L., Hager, B.H., Lee, D.C., and Wiechert, U. (2006). Thermal and magmatic evolution of the Moon. In Joliff, B.L., Wieczorek, M.A., Shearer, C.K., and Neal, C.R. (Eds). New views of the Moon, Reviews in Mineralogy and Geochemistry, 60, pp. 365-469.

Shearer, C.K., Papike, J.J., and Karner, J.M. (2006). Pyroxene europium valence oxybarometer: Effects of pyroxene composition, melt composition, and crystallisation kinetics. American Mineralogist 91: 1565-1573.

Shoemaker E.M., Batson R.M., Bean A.L., Conrad C.Jr., Dahlem D.H., Goddard E.N., Hait M.H., Larson K.B., Schaber G.G., Schleicher D.L., Sutton R.L., Swann G.A., and Waters A. C. (1970). Preliminary geologic investigation of the Apollo 12 Landing site. Part A. Geology of the Apollo 12 landing site. P113-156, Apollo 12 Preliminary Science report, NASA SP-235.

Simon, S. B., Papike, J. J., Gosselin, D. C., and Laul, J. C. (1985). Petrology and chemistry of Apollo 12 regolith breccias. Journal of Geophysical Research 90 (SO1): 75-86.

Simpson,, P.R., and Bowie, S.H.V. (1971). Opaque phases in Apollo 12 samples. Proceedings, 2nd Lunar and Planetary Science Conference:207-218.

Snape, J.F., Crawford, I.A., Joy, K.H., and Burgess, R. (2011a). A petrographic study of basalt fragments in Apollo regolith sample 12003 (abstract #2020). 42nd Lunar & Planetary Science Conference.

Snape, J.F., Beaumont, S., Burgess, R., Crawford, I.A., and Joy, K.H. (2011b). An evaluation of techniques used in the age and petrologic analysis of Apollo 12 basalts (abstract #2011). 42nd Lunar & Planetary Science Conference.

Snape, J.F., Joy, K.H., and Crawford, I.A. (2011c). Characterization of multiple lithologies within the lunar feldspathic regolith breccia meteorite Northeast Africa 001. Meteoritics & Planetary Science 46: 1288 – 1312.

Snape, J.F. Joy, K.H., Crawford, I.A., and Alexander, L. (2014, In press). Basaltic diversity at the Apollo 12 site: inferences from petrologic examinations of the soil sample 12003. Meteoritics and Planetary Science.

Snape, J.F., Alexander, L., Crawford, I.A., and Joy, K.H. (2013). Basaltic regolith sample 12003,314: A new member of the Apollo 12 Feldspathic basalt suite? (abstract #1044). 44th Lunar & Planetary Science Conference. CD-ROM.

Snyder, G.A., Neal, C.R., Taylor, L.A., and Halliday, A.N. (1997). Anatexis of lunar cumulate mantle in time and space: Clues from trace-element, strontium, and neodymium isotopic chemistry of parental Apollo 12 basalts. Geochimica et Cosmochimica Acta 61: 2731-2747.

Taylor, L.A., Kullerud, G., and Bryan, W.B. (1971). Opaque mineralogy and textural features of Apollo 12 samples and a comparison with Apollo 11 rocks. Proceedings, 2nd Lunar and Planetary Science Conference: 855-871.

USGS (2009), Basalt, Columbia River, BCR-2. U.S. Geological Survey Certificate of Analysis, http://minerals.cr.usgs.gov/geo_chem_stand/basaltbcr2.html

Vaniman, D.T., Dietrich, J., Taylor, G.J., and Heiken, G.H. (1991). Exploration, samples and recent concepts of the Moon. In Heiken, G.H., Vaniman, D.T., French, B.M. (Eds). *Lunar Sourcebook*, Cambridge University Press pp.5-26.

Warren, P.H. (1997). The unequal host-phase density effect in electron probe defocused beam analysis: An easily correctable problem. (Abstract #1497). 28th Lunar & Planetary Science Conference. CD-ROM.

Weill, D.F., Grieve, R.A., McCallum, I.S., and Bottinga, Y. (1971). Mineralogy-petrology of lunar samples. Microprobe studies of samples 12021 and 12022; viscosity of melts of selected lunar compositions. Proceedings, Lunar and Planetary Science Conference: vol.2, p.413.

Zeigler, R.A., Korotev, R.L., Haskin, L.A., Jolliff, B.L., and Gillis, J.J., (2006). Petrography and geochemistry of five new Apollo 16 mare basalts and evidence for post-basin deposition of basaltic material at the site. Meteoritics & Planetary Science 41: 263 – 284.

Figures

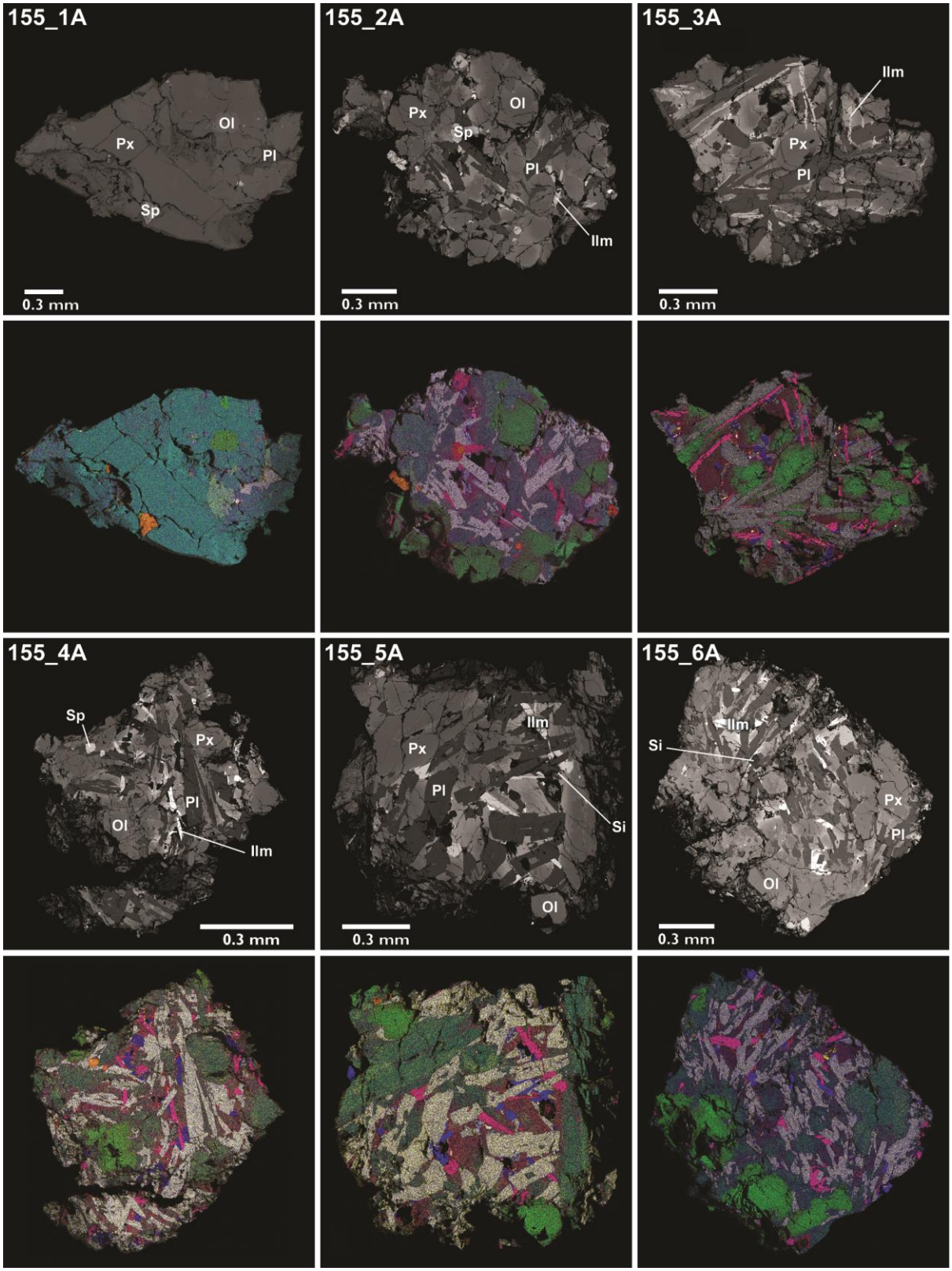

Figure 1. Backscattered electron (BSE) images and false colour element maps of samples 155_1A to 6A. Colours on the element maps represent concentrations of different elements as follows: Si = blue, Fe = red, Mg = green, Ca = yellow, Al = white, Ti = pink and Cr= gold. Abbreviations on BSE images correspond to the following: Pyroxene (Px), olivine (Ol), plagioclase (Pl), ilmenite (Ilm), silica (Si) and spinel (Sp).

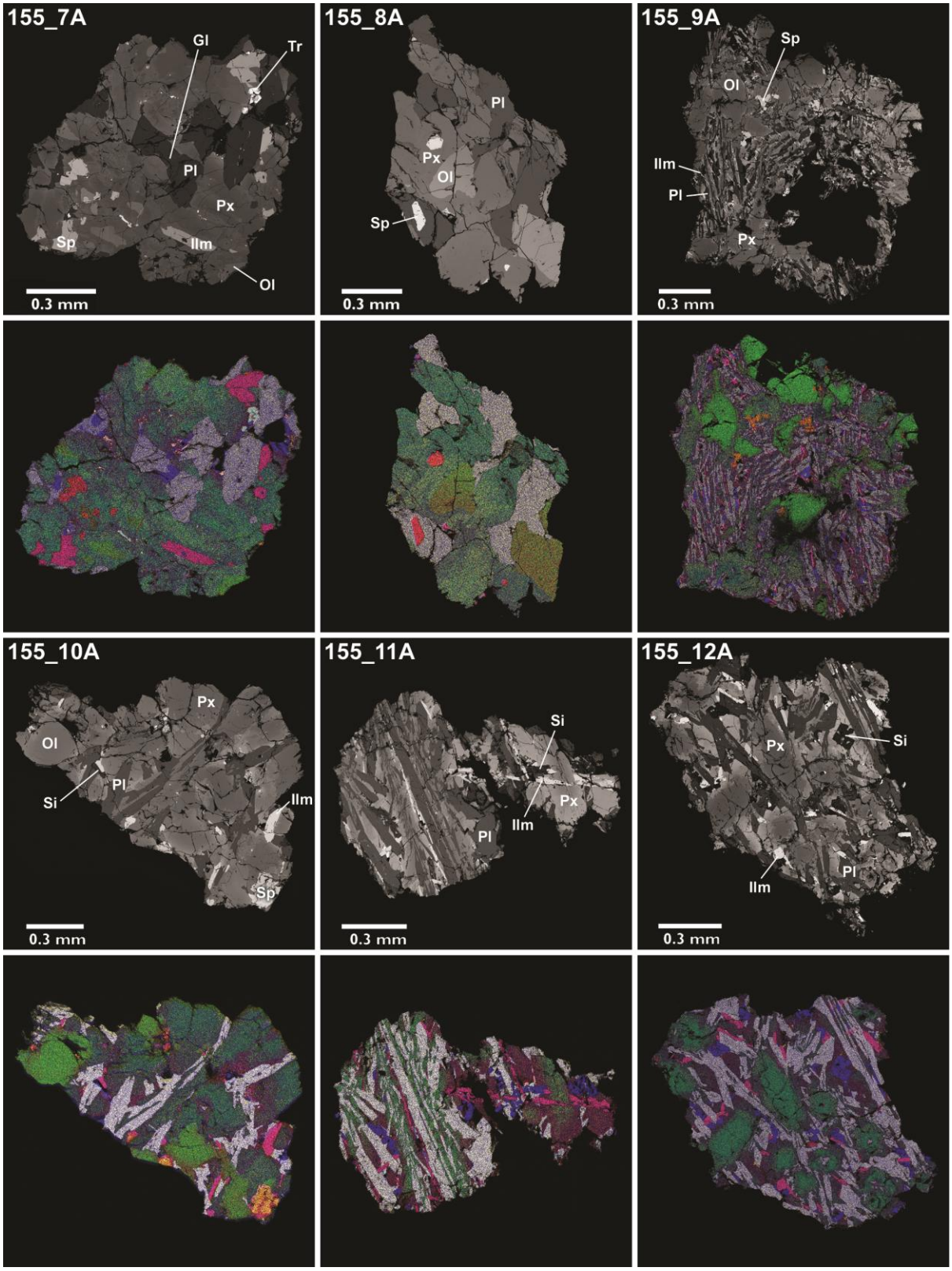

Figure 2. Backscattered electron (BSE) images and false colour element maps of samples 155_7A to 12A. Colours on the element maps represent concentrations of different elements as follows: Si = blue, Fe = red, Mg = green, Ca = yellow, Al = white, Ti = pink and Cr = gold, and S = light blue in 155_7A only to highlight the increased modal abundance of sulfides in this sample. Abbreviations on BSE images correspond to the following: Pyroxene (Px), olivine (Ol), plagioclase (Pl), ilmenite (Ilm), silica (Si), spinel (Sp), troilite (Tr) and glass (Gl).

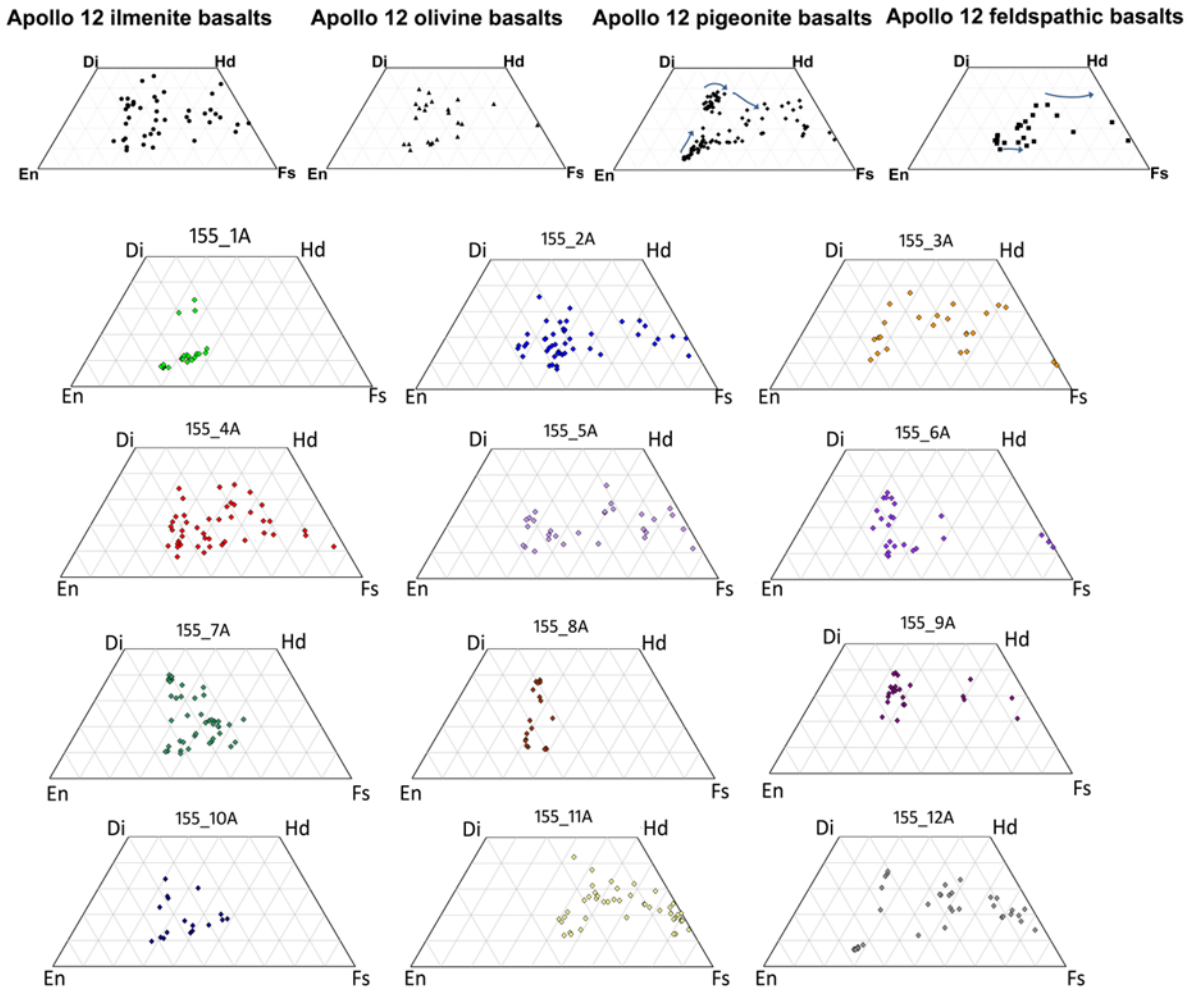

Fig. 3. Pyroxene quadrilateral plots showing pyroxene compositions in previously published Apollo 12 basalt groups, with evolutionary trends indicated from Papike et al., 1976, together with the individual pyroxene compositions from 12023,155 obtained in this work. Apollo 12 basalt data from Brett et al., 1971; Weil et al, 1971; Hollister et al., 1971; Bence et al., 1970; Dence et al., 1971; Kushiro et al., 1971; Newton et al., 1971; Anderson and Smith, 1971; Brown et al., 1971; Beaty et al., 1979; Dungan and Brown, 1977; Baldridge et al., 1979 and this study (pyroxene compositions from 12038).

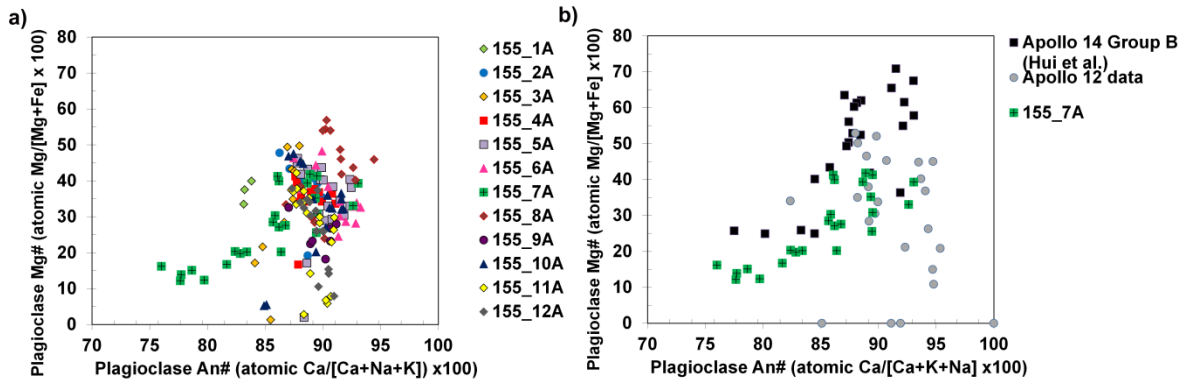

Figure 4. Variation of An# (atomic Ca/[Ca+Na+K]) with Mg# (atomic Mg/[Mg+Fe]) in plagioclase. a) in all 12023,155 samples in this study and b) in 12023,155_7A compared with Apollo 12 data (Crawford, 1973; Drake et al., 1970; Keil et al., 1971; Lunatic Asylum, 1970; Newton et al., 1971; Taylor et al., 1971; Weill et al., 1971) and Group B Apollo 14 basalts (Hui et al., 2011). These plots illustrate the difference in crystallisation trend for 12023,155_7A with other Apollo 12 basalts and samples in this study, and the similarity between 155_7A and Apollo 14 Group B basalts.

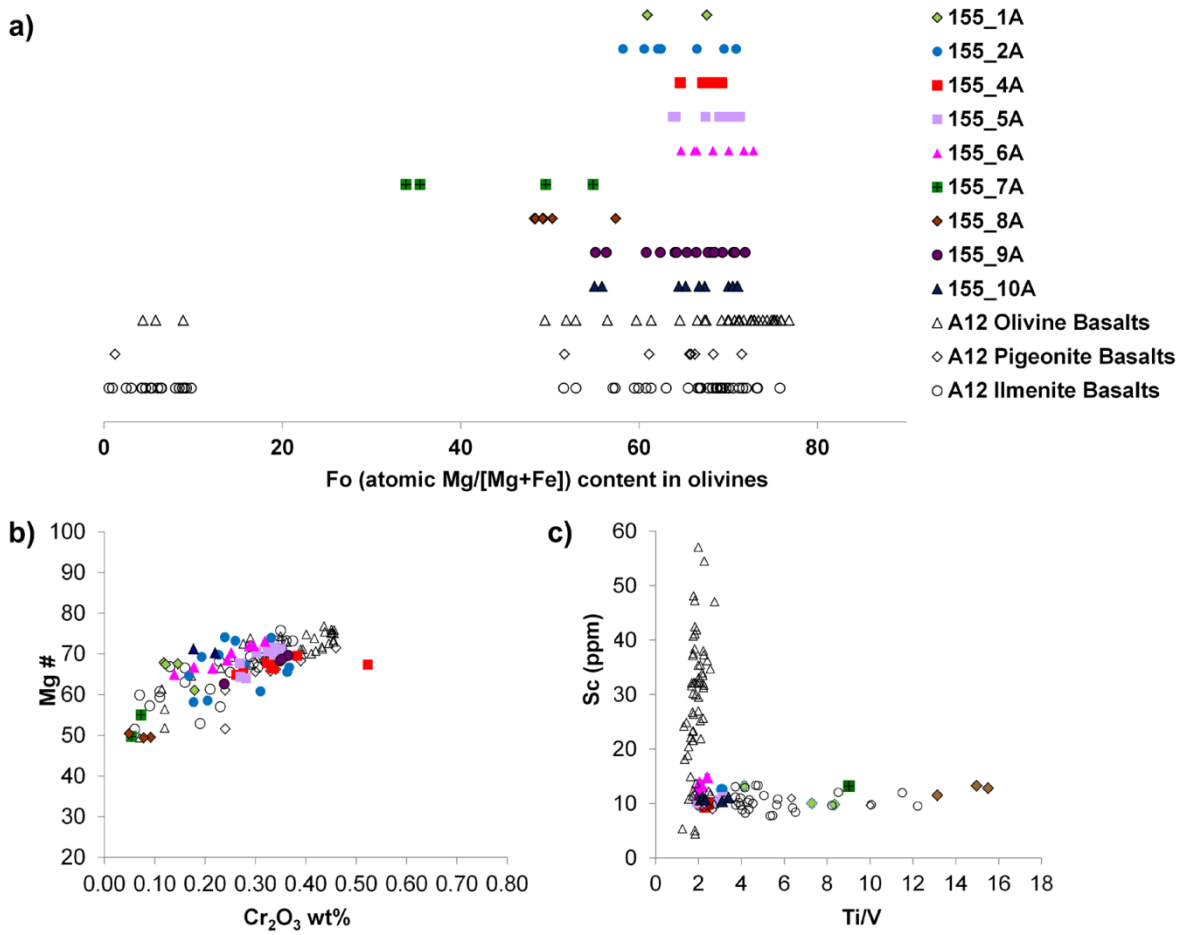

Figure 5. Olivine compositions in 12023,155. a) Fo (atomic Mg/(Mg+Fe) contents in olivine. Comparative data is given for Apollo 12 olivine, pigeonite and ilmenite basalts. Data sources are: Bence et al., 1970; Brett et al., 1971; Brown et al., 1971; Baldridge et al., 1979; Butler, 1972; El Goresy et al., 1971; Dungan and Brown, 1977; Hollister et al., 1971; Keil et al., 1971; Kushiro et al., 1971; Newton et al., 1971; and Weill et al., 1971. b) Comparison of Mg# (atomic Mg/[Mg + Fe]) to Cr_2O_3 in Mg-rich olivine in 12023,155. Olivine plotted all have Mg#>55 with the exception of 155_7A and 155_8A which do not have any forsteritic olivine. Comparative data as for (a). c) Sc (ppm) vs. Ti/V (ppm) in olivine. Comparative data from Fagan et al.(2013).

Tables

Modal Mineralogy Calculations (%) 12023,155.												
	1A	**2A**	**3A**	**4A**	**5A**	**6A**	**7A**	**8A**	**9A**	**10A**	**11A**	**12A**
Ilmenite	1.4	3.0	4.2	4.9	3.2	2.6	6.5	0.2	7.3	2.3	4.5	4.2
Chromite/ Ulvöspinel		0.7		trace		0.2	1.0	1.3	0.5	1.6		
Olivine	2.0	11.9		4.8	2.8	5.9	1.9	13.9	7.8	13.0		
Pyroxene	93.9	53.7	47.6	41.2	54.5	56.7	67.6	55.6	43.8	61.9	43.5	60.2
Feldspar	2.7	30.7	44.6	42.3	36.6	29.9	21.9	28.9	36.9	19.3	42.8	31.0
Silica			3.6	6.8	2.9	4.7	1.1	0.1	3.7	1.9	9.2	4.6
Total	100.0	100.0	100.0	100.0	100.0	100.0	100.0	100.0	100.0	100.0	100.0	100.0

Table 1. Modal mineralogies of basalt fines from lunar soil sample 12023,155. Modal mineralogies are calculated from BSE images and elemental maps using a pixel counting method detailed in section 2. Values are normalised to 100%. Based on multiple pixel counts of the same sample, absolute uncertainties on these modal abundances are typically in the range of 0 to 5%.

Sample	**155_1A**	**155_2A**	**155_3A**	**155_4A**	**155_5A**	**155_6A**
Na_2O	0.31 ± 0.02	0.42 ± 0.01	0.55 ± 0.02	0.46 ± 0.01	0.50 ± 0.02	0.42 ± 0.02
MgO	20.28 ± 0.03	12.72 ± 0.12	6.34 ± 0.04	7.47 ± 0.08	7.83 ± 0.02	10.29 ± 0.02
Al_2O_3	2.31 ± 0.03	8.66 ± 0.17	10.65 ± 0.07	11.91 ± 0.08	12.29 ± 0.26	10.61 ± 0.10
SiO_2	51.48 ± 0.06	43.86 ± 0.10	44.31 ± 0.03	45.30 ± 0.09	46.54 ± 0.23	44.12 ± 0.08
K_2O	0.01 ± 0.02	0.07 ± 0.01	0.07 ± 0.01	0.07 ± 0.01	0.12 ± 0.02	0.09 ± 0.02
CaO	5.10 ± 0.01	8.05 ± 0.06	10.80 ± 0.06	10.50 ± 0.06	10.21 ± 0.01	9.66 ± 0.02
TiO_2	0.90 ± 0.04	3.05 ± 0.08	5.69 ± 0.08	3.95 ± 0.07	3.65 ± 0.08	3.26 ± 0.05
FeO	19.18 ± 0.07	23.06 ± 0.16	21.65 ± 0.12	19.07 ± 0.08	17.67 ± 0.01	20.67 ± 0.03
Total	99.56	99.89	100.06	98.73	98.81	99.13
Mg #	65.33 ± 0.21	49.58 ± 0.52	34.30 ± 0.27	41.12 ± 0.19	44.13 ± 1.65	47.02 ± 0.51
weight (g)	0.0028	0.0024	0.0029	0.0046	0.0038	0.0029
Sample	**155_7A**	**155_8A**	**155_9A**	**155_10A**	**155_11A**	**155_12A**
Na_2O	0.38 ± 0.01	0.46 ± 0.02	0.44 ± 0.01	0.51 ± 0.01	0.49 ± 0.02	0.43 ± 0.02
MgO	10.17 ± 0.01	12.26 ± 0.06	12.54 ± 0.23	14.41 ± 0.09	3.71 ± 0.04	6.99 ± 0.04
Al_2O_3	5.56 ± 0.08	9.84 ± 0.15	8.67 ± 0.15	7.13 ± 0.09	11.57 ± 0.09	10.52 ± 0.07
SiO_2	44.21 ± 0.11	45.88 ± 0.11	42.11 ± 0.15	45.22 ± 0.16	43.78 ± 0.17	46.89 ± 0.12
K_2O	0.14 ± 0.07	0.03 ± 0.01	0.05 ± 0.01	0.05 ± 0.01	0.14 ± 0.01	0.09 ± 0.01
CaO	9.69 ± 0.01	10.39 ± 0.07	8.01 ± 0.13	8.14 ± 0.07	10.91 ± 0.05	10.65 ± 0.06
TiO_2	5.18 ± 0.09	1.32 ± 0.06	3.25 ± 0.05	2.51 ± 0.07	5.29 ± 0.12	2.93 ± 0.06
FeO	24.91 ± 0.03	19.43 ± 0.16	23.83 ± 0.19	21.62 ± 0.16	23.96 ± 0.14	19.70 ± 0.11
Total	100.24	99.61	98.88	99.59	99.84	98.20
Mg #	42.12 ± 0.39	52.94 ± 0.34	48.40 ± 1.12	54.30 ± 0.40	21.63 ± 0.24	38.74 ± 0.28
weight (g)	0.0024	0.0018	0.0059	0.0032	0.0038	0.0014

Table 2. Bulk chemical compositions in wt% oxide for samples 12023,155 fragments_1A to _12A. Mg# = Mg/(Mg+Fe) atomic x100. Errors for major element oxides are 1δ standard deviation calculated from the repeat raster beam analyses. Propagation of errors is used to calculate the error for Mg#. Weights for the samples are given in g.

Sample	Most primitive measured olivine Mg#	Predicted equilibrium melt Mg#	Measured bulk rock Mg#	Predicted equilibrium olivine Mg#
155_1A	67.8	41.1	65.3	85.1
155_2A	74.1	48.6	49.6	74.9
155_4A	69.4	42.8	41.1	67.9
155_5A	71.2	45.0	44.1	70.5
155_6A	73.1	47.3	47.0	72.9
155_7A	55.0	28.8	42.1	68.8
155_8A	50.5	25.2	52.9	77.3
155_9A	72.1	46.1	48.4	74.0
155_10A	71.2	45.0	54.3	78.3

Table 3. Modelled equilibrium parent melt Mg# from olivine compositions and predicted melt Mg# from the bulk chemistry of samples 12023,155_1A, 2A, 4A, 5A, 6A, 7A, 8A, 9A and 10A (n.b. samples not modelled do not contain olivine).